



Article

# Optimization of Two Soil–Structure Interaction Parameters Using Dynamic Centrifuge Tests and an Analytical Approach

Hyun-Uk Kim <sup>1,2</sup>, Jeong-Gon Ha <sup>3</sup>, Kil-Wan Ko <sup>2</sup> and Dong-Soo Kim <sup>2,\*</sup>

<sup>1</sup> R&D Strategy and Planning Office, Central Research Institute of Korea Hydro and Nuclear Power (KHNP), Daejeon 34101, Korea; gomzee@kaist.ac.kr

<sup>2</sup> Department of Civil and Environmental Engineering, Korea Advanced Institute Science and Technology (KAIST), Daejeon 34141, Korea; kwko@kaist.ac.kr

<sup>3</sup> Structural Safety & Prognosis Research Division, Korea Atomic Energy Research Institute (KAERI), Daejeon 34057, Korea; jgha87@kaist.ac.kr

\* Correspondence: dskim@kaist.ac.kr; Tel.: +82-42-350-3619

Received: 14 July 2020; Accepted: 31 August 2020; Published: 31 August 2020



**Abstract:** The response of the structure subjected to an earthquake load is greatly affected by the properties of the structure and soil so it is very important to accurately determine the characteristics of the structure and soil for analysis. However, studies on the effective profile depth where soil properties are determined, have been conducted in the presence of restricted conditions (i.e., surface foundation, linear soil properties), and without any considerations on damping. In case of the effective height of structure that affects its rocking behavior, it was only theoretically or empirically determined. In addition, most previously published studies on soil–structure interaction (SSI) focused on limited effects and parameters (e.g., rocking behavior, embedment effect, effective profile depth, spring constant, and damping coefficient) and not on comprehensive SSI parameters. Furthermore, no detailed validation procedure has been set in place which made it difficult to validate the SSI parameters. Since the effective height of structure and effective profile depth are the basis of all the input parameters of SSI analysis, it is important to validate and determine them. Therefore, in this study, the procedure used to optimize the two SSI parameters was established based on an analytical approach that considered all the possible SSI parameters that were investigated from conventional codes and studies and physical model tests. As a result of this study, the optimum values of the effective height of the structure and effective profile depth were respectively determined according to (a) the height from the bottom part of the foundation to the center of the mass of the superstructure, and according to (b) the depth at values equal to four times the radius of the foundation.

**Keywords:** effective height; effective profile depth; SSI; analytical approach; centrifuge test

## 1. Introduction

The dynamic characteristics of the structure depend on the surrounding soil. To estimate an accurate structural response for seismic design, the soil–structure interaction (SSI) effect has been considered as the crucial effect for the seismic evaluation of the structure. There have been various studies on the soil–structure interaction (SSI) effect but the subject of each study was not comprehensive but limited to specific parameters or phenomena (e.g., spring constant and damping coefficient [1–6], effective profile depth [7], and rocking behavior [8–11]). With regard to the SSI analysis, four procedures were introduced in FEMA356 [12]: Linear static procedure (LSP), linear dynamic procedure (LDP), nonlinear static procedure (NSP), and nonlinear dynamic procedure (NDP). Among them, the static procedures (i.e., LSP and NSP) have been accepted in various standards owing to their simplicity and

practicality [12–15], and the dynamic procedures (i.e., LDP and NDP) have been used to either verify the static procedures or to obtain more detailed structural responses. Even though all the standards mentioned above (i.e., FEMA 356, ATC-40, FEMA 440, and ASCE 41–13) define the same three types of modes (i.e., structural swaying, foundation swaying, and rocking), the formula for the soil–spring constant and damping coefficient, and the two SSI parameters (i.e., the effective height of the structure and effective profile depth) were defined differently at various standards and studies, including the aforementioned standards [1–4,7,12,14,16–19]. The two SSI parameters are very important because they determine the dynamic soil properties and the rocking potential of the soil–structure system (i.e., rocking damping coefficient and moment), but they have been derived in restricted conditions (i.e., the effective profile depth was determined based only on considerations of static soil stiffness in surface foundation condition [5,7]) and theoretically determined (i.e., the effective height was determined based on structural dynamic theory [3,10,12,13]). In addition, existing standards and prior studies have been limited in view of the following: (1) Approximate consideration of the nonlinear deformation characteristics of the soil based on peak ground acceleration [12,14,15,18], (2) determination of damping ratio of soil based only on radiation damping considerations [14,15,18], and (3) lack of detailed SSI analysis procedure and SSI parameter validation procedure with physical model tests. Therefore, in this study, the optimum SSI parameter selection procedure was established using an LDP-based analytical approach and relevant tests, whereby the SSI effects were comprehensively and appropriately considered (i.e., consideration of all the possible SSI parameters for analysis, accurate consideration of soil nonlinearity using site response analysis, and determination of total soil damping coefficient, including soil material damping). Finally, two optimum SSI parameters were determined based on a number of analyses according to the established procedure.

## 2. Soil–Structure Interaction (SSI) Parameters and Optimum SSI Parameter Selection Procedure

The SSI model is shown in Figure 1. It consists of two lumped masses  $m_s$  and  $m_f$ , whereby the distance between the two masses is defined as the effective height  $h$ , a set of spring  $k_s$ , and dashpot  $C_s$  to represent the dynamic characteristics of the structure, and two sets of springs and dashpots to simulate the flexibility and damping of the soil. In the case of horizontal excitation, the total absolute displacement  $x$  of the  $m_s$  can be defined with three deformation modes, and is expressed as  $x = x_g + u_x + h\varnothing + u_s$ . In this case,  $x_g$  is the absolute displacement of the soil,  $u_x$  is the relative displacement between the foundation and the soil,  $\varnothing$  is the rotation angle of the foundation,  $h$  is the effective height of the structure, and  $u_s$  is the relative displacement between the upper structure and the soil, or the net structural displacement.

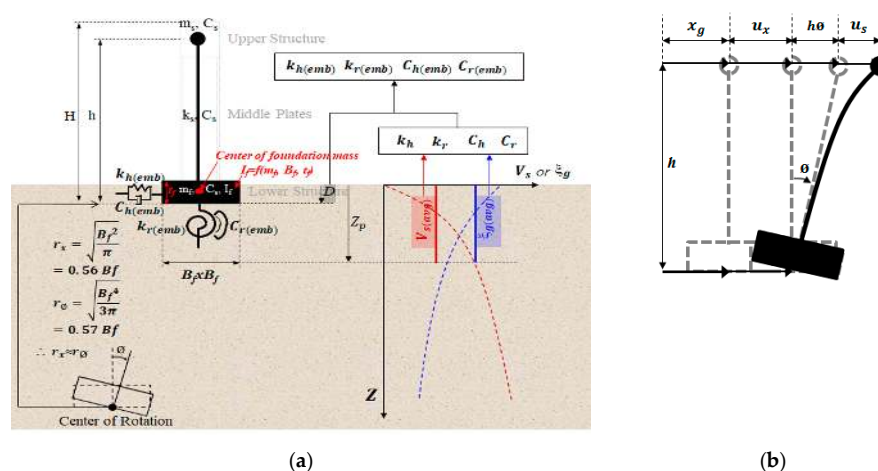


**Figure 1.** Three degree-of-freedom (3DOF) idealization of soil–structure system and each displacement mode: (a) 3DOF idealization for soil–structure interaction (SSI) analysis, and (b) displacement according to each mode.

To obtain detailed structural responses, the equation of motion (EOM) of the soil–structure system that considers the aforementioned three degree-of-freedom (3DOF) is expressed by Equation (1) [8,9,20].

$$\begin{bmatrix} m_s & m_s & m_s h \\ m_s & m_s + m_f & m_s h \\ m_s h & m_s h & m_s h^2 + I_f \end{bmatrix} \begin{Bmatrix} \ddot{u}_s \\ \ddot{u}_x \\ \ddot{\phi} \end{Bmatrix} + \begin{bmatrix} c_s & 0 & 0 \\ 0 & c_x & 0 \\ 0 & 0 & c_\phi \end{bmatrix} \begin{Bmatrix} \dot{u}_s \\ \dot{u}_x \\ \dot{\phi} \end{Bmatrix} + \begin{bmatrix} k_s & 0 & 0 \\ 0 & k_x & 0 \\ 0 & 0 & k_\phi \end{bmatrix} \begin{Bmatrix} u_s \\ u_x \\ \phi \end{Bmatrix} = -\ddot{x}_g \begin{Bmatrix} m_s \\ m_s + m_f \\ m_s h \end{Bmatrix} \quad (1)$$

### 2.1. Soil–Spring Constants and Damping Coefficients

In the SSI system, the soil–spring constant and damping coefficient represent the characteristics of the foundation and lower ground, and impose a considerable influence on the system’s response. Regarding the soil–spring constant and damping coefficient, Wolf [1] and Richart and Lysmer [2] suggested the use of the frequency-independent spring constant and radiation damping coefficient formulas that comprised simple parameters. These formulas have been used previously [14,19,21]. Gazetas [3] and Stewart et al. [4] proposed a precise frequency-dependent spring constant and damping coefficient formula that considered the soil impedance. However, to utilize the formulas, it is necessary to consider numerous parameters and numerous corrections for each frequency subject to earthquake loading. In FEMA356 [12], the frequency-independent soil stiffness and correction factor formulas—that considered the geometry and embedment depth of the rectangular footing in detail—were presented, but the damping coefficient formula was not presented. Therefore, two types of simple frequency-independent soil–spring constant and radiation damping coefficient formulas have been presented in Table 1 (i.e., the formulas suggested by Wolf [1] and Richart and Lysmer [2]) were adopted in this study.

**Table 1.** Soil–spring constant and radiation damping coefficient for surface foundation.

Type of Formula	Spring Constant		Radiation Damping Coefficient	
	$K_x (=k_h)$	$K_\phi (=k_r)$	$C_x$	$C_\phi$
Wolf [1] FEMA440 [14]	$\frac{8Gr_x}{2-v}$	$\frac{8Gr_\phi^3}{3(1-v)}$	$\frac{4.6}{2-v}\rho V_s r_x^2$	$\frac{0.4}{1-v}\rho V_s r_\phi^4$
Richart and Lysmer [2], EPRI [19], ASCE4-16 [21]	$2(1+v)G\beta_x \sqrt{BL}$	$\frac{G}{1-v}\beta_\phi BL^2$	$0.576 k_x r_x \sqrt{\frac{\rho}{G}}$	$\frac{0.3}{1+B_\phi} k_\phi r_\phi \sqrt{\frac{\rho}{G}}$

Where  $B$  is the width of the foundation,  $L$  is the length of the foundation,  $G$  is the shear modulus of the soil,  $\nu$  is the Poisson’s ratio of the soil, and  $r_x$  and  $r_\phi$  are the equivalent radii of the foundation expressed as  $\sqrt{BL/\pi}$  and  $\sqrt[4]{BL^3/3\pi}$ , respectively. The parameters  $\beta_x$  and  $\beta_\phi$  are a function of  $L/B$ , and the values in case of square footing (i.e.,  $L/B = 1$ ) can be obtained from the suggested chart, where  $\beta_x$  and  $\beta_\phi$  are equal to 1 and 0.5, respectively.

#### 2.1.1. Strain-Dependent Soil Properties

Linear SSI analyses (i.e., LSP and LDP) require constant soil properties regardless of depth and strain, but the actual shear wave velocity of soil  $V_s$  ( $V_s$ ) and damping ratio of soil  $\xi_g$  ( $\xi_g$ ) vary with depth and strain level. In conventional standards, the reduction factor for  $V_s$  is determined and used to convert the strain dependent  $V_s$  to a strain-independent factor, but a reduction factor is expressed as a function of the peak ground acceleration at the ground surface without considering the frequency contents of motion and depth. Moreover, there is no correction factor for  $\xi_g$  in the standards [12,14,15,18]. To overcome the above limitation and to obtain strain-independent  $V_s$  and  $\xi_g$  values (i.e., equivalent  $V_s$  and  $\xi_g$  values) accurately during the excitation, one-dimensional equivalent linear-site-response analyses (SRAs) were performed in this study.

### 2.1.2. Depth-Dependent Soil Properties and Effective Profile Depth ( $Z_p$ )

Although equivalent  $V_s$  and  $\xi_g$  values are converted to their strain-independent forms, they are still non-uniformly distributed as a function of depth. Therefore, it is necessary to define an effective profile depth ( $Z_p$ ). In this way, depth-independent, equivalent  $V_s$  and  $\xi_g$  values have to be obtained as the average values within a depth  $Z_p$ . The averaged values of  $V_s$  and  $\xi_g$  that consider  $Z_p$  can be obtained by Equation (2), as follows,

$$V_{s(avg)} = \frac{Z_p}{\sum_{i=1}^n \frac{\Delta Z_i}{(V_s)_i}}, \quad \xi_{g(avg)} = \frac{Z_p}{\sum_{i=1}^n \frac{\Delta Z_i}{(\xi_g)_i}} \quad (2)$$

where  $(V_s)_i$  is the shear wave velocity of the  $i$ th soil layer,  $(\xi_g)_i$  is the material damping ratio of the  $i$ th soil layer, and  $\Delta Z_i$  is the thickness of the  $i$ th soil layer, respectively. Stewart et al. [7] regarded the static soil–spring constants obtained from the impedance solutions by Wong and Luco [5] as reference values, and repeatedly calculated the soil–spring constants at various profile depths. Note that  $Z_p$  is 0.75 times the radius of the foundation ( $r$ ), wherein the residual between the reference and the calculated value is minimized. In addition to prior research publications, in the recommended provision of national earthquake hazard reduction program (NEHRP) [16],  $4r$  and  $1.5r$  were proposed as the respective values of  $Z_p$  for swaying and rocking behaviors, respectively. However, in previous studies, the embedment effect and damping ratio of soil were not considered. Therefore, in this study, three types of scenarios of  $0.75r$ ,  $2r$ , and  $4r$ , were considered to evaluate the optimum effective profile depth and necessary considerations (i.e., embedment effect and  $\xi_g$ ), and were included in the analytical approach for the evaluation of the optimum effective profile depth.

### 2.1.3. Embedment Correction for Spring Constant and Radiation Damping Coefficient

When the foundation was embedded, the natural frequency of the soil–structure system increased owing to an increase in the soil stiffness, and the overall response of the system decreased owing to an increase in radiation damping [22]. In view of this phenomenon, the formulas of the correction factor that considered the geometry and embedment depth of the rectangular footing in detail was presented in FEMA356 [12]. In contrast, Whitman [6] proposed a simple embedment correction factor (i.e., correction factor for both stiffness and damping) as a function of the embedment depth ( $D$ ), radius of foundation ( $r$ ), and Poisson’s ratio ( $\nu$ ) of the soil. Table 2 shows the correction factor for embedment suggested by Whitman. According to the Whitman’s suggestion, the damping correction factor was suggested for the radiation damping ratio of the soil but the damping matrix in Equation (1) needed a damping coefficient ( $C_x$  and  $C_\phi$ ). Therefore, the correction factor formula was converted to Equation (3) and was used in this study, wherein  $C_{x(emb)}$  and  $C_{\phi(emb)}$  are expressed as  $\alpha_x \sqrt{\eta_x} c_x$  and  $\alpha_\phi \sqrt{\eta_\phi} c_\phi$ , respectively.

**Table 2.** Correction factor for embedment and corrected soil properties [6].

Property	Mode	Correction Factor for Embedment	Corrected Stiffness and Damping Ratio
stiffness	swaying ( $x$ )	$\eta_x = 1 + 0.55(2 - \nu) \frac{D}{r_x}$	$k_{x(emb)} = \eta_x \cdot k_x$
	rocking ( $\phi$ )	$\eta_\phi = 1 + 1.2(1 - \nu) \frac{D}{r_\phi} + 0.2(2 - \nu) \frac{D^3}{r_\phi^3}$	$k_{\phi(emb)} = \eta_\phi \cdot k_\phi$
radiation damping	swaying	$\alpha_x = \left[ 1 + 1.9(2 - \nu) \frac{D}{r_x} \right] / \sqrt{\eta_x}$	$\xi_{x(emb)} = \alpha_x \cdot \xi_x$
	rocking	$\alpha_\phi = \left[ 1 + 0.7(1 - \nu) \frac{D}{r_\phi} + 0.6(2 - \nu) \frac{D^3}{r_\phi^3} \right] / \sqrt{\eta_\phi}$	$\xi_{\phi(emb)} = \alpha_\phi \cdot \xi_\phi$

$$\begin{aligned}
 C_{x(emb)} &= C_{cr\ x(emb)} \xi_{x(emb)} = 2 \sqrt{m_t k_{x(emb)}} \xi_{x(emb)} = 2 \sqrt{m_t k_{x(emb)}} \left( \alpha_x \frac{C_x}{2 \sqrt{m_t k_x}} \right) = \alpha_x \sqrt{\eta_x} C_x \\
 C_{\varnothing(emb)} &= C_{cr\ \varnothing(emb)} \xi_{\varnothing(emb)} = 2 \sqrt{I_0 k_{\varnothing(emb)}} \xi_{\varnothing(emb)} = 2 \sqrt{I_0 k_{\varnothing(emb)}} \left( \alpha_{\varnothing} \frac{C_{\varnothing}}{2 \sqrt{I_0 k_{\varnothing}}} \right) = \alpha_{\varnothing} \sqrt{\eta_{\varnothing}} C_{\varnothing}
 \end{aligned}
 \tag{3}$$

#### 2.1.4. Determination of Soil Damping Based on Radiation and Material Damping Considerations

The total damping coefficient formula consists of the material damping and the radiation damping coefficients [1,3,19]. Assuming that the structure is rigid ( $k_s = \infty$ ) and that the foundation cannot rock ( $k_r = \infty$ ), or is only allowed to rock ( $k_h = \infty$ ), the natural frequency of each case follows  $\omega_h^2 = k_h/m_t$  and  $\omega_r^2 = k_r/I_0$  [1], where  $m_t$  and  $I_0$  are the total mass and total mass moment of inertia of the structure, respectively. Equation (4) expresses a form of the total damping coefficient based on the consideration of the embedment effect. Substituting the natural frequency equation in each mode in Equation (4) estimates the swaying and rocking total damping coefficients, as listed in Table 3, wherein  $C_{gx}$  and  $C_{g\phi}$  are the respective swaying and rocking material damping coefficients. The total damping coefficient was expressed as function of  $C_h$  and  $C_r$  to distinguish them from the subscripts  $x$  and  $\phi$  of the radiation damping coefficient. Accordingly, the soil–spring constant was also denoted by  $k_h$  and  $k_r$  for the swaying and rocking modes.

$$C_{(emb)} = \text{radiation } C_{(emb)} + \text{material } C_{g(emb)} = C_{(emb)} + \frac{2}{\omega_{(emb)}} \xi_g k_{(emb)}
 \tag{4}$$

**Table 3.** Soil–spring constant and total damping coefficient formulas based on embedment effect considerations.

Property	Mode	Soil–Spring Constant and Damping Coefficient Formula
soil spring constant	swaying ( $h$ )	$k_{h(emb)} = k_{x(emb)} = \eta_x \cdot k_x$
	rocking ( $r$ )	$k_{r(emb)} = k_{\varnothing(emb)} = \eta_{\varnothing} \cdot k_{\varnothing}$
soil total damping coefficient	swaying	$C_{h(emb)} = C_{x(emb)} + C_{gx(emb)} = \alpha_x \sqrt{\eta_x} c_x + 2 \sqrt{m_t k_{x(emb)}} \xi_g$
	rocking	$C_{r(emb)} = C_{\varnothing(emb)} + C_{g\varnothing(emb)} = \alpha_{\varnothing} \sqrt{\eta_{\varnothing}} c_{\varnothing} + 2 \sqrt{I_0 k_{\varnothing(emb)}} \xi_g$

#### 2.2. Effective Height of Structure $h$

In the soil–structure system, the effective height ( $h$ ) of the structure affects its rocking response of the system. Stewart et al. [17] defined  $h$  as the distance from the foundation to the centroid of the inertial force in relation to the fundamental mode. In FEMA440 [14] and FEMA450 [18], the full height was considered as the value of  $h$  of the one-story structure, and the distance from the foundation to the center point of the first modal shape was set to  $h$  in multistory structures. In the Electric Power Research Institute (EPRI) training module [19],  $h$  was calculated based on the moment equilibrium to the center of mass of the rigid foundation. According to the recent research by Gavras et al. [10], the value of  $h$  of the footing–flexible column–bridge deck system was defined as the distance from the base of the footing to the center of the deck. However, a limited number of studies have verified or validated the optimum effective height of the structure. In this study, three effective heights ( $h$ ) were considered to choose the optimum  $h$ , whereby the two heights were suggested by conventional standards, and the other height satisfied the total mass moment of inertia ( $I_0$ ) of the structure. The three effective heights used in this study adhered to the following order: Height from the bottom of the foundation to the center of mass of the superstructure ( $h_{base\ to\ m_s}$ ) < height compatible to the total mass moment of inertia of the structure ( $h_{MMI}$ ) < height needed to satisfy moment equilibrium ( $h_{moment}$ ). Additionally,  $h_{MMI}$  and  $h_{moment}$  can be obtained as indicated below,

$$h_{MMI} = (I_0 - I_f/m_s)^{0.5}
 \tag{5}$$

$$h_{moment} = M_0 - M_f/m_{sg}
 \tag{6}$$

where  $I_0$  is the total mass moment of inertia of the upper, middle, and lower structures, and  $I_f$  is the mass moment of inertia based on the consideration of the effective mass  $m_f$  and the geometry of foundation,  $M_0$  is the summation of the moment of the upper, middle, and lower structures, and  $M_f$  is the moment that considers the effective mass  $m_f$  and the geometry of the foundation.

### 2.3. Procedure Used to Identify the Optimum $Z_p$ and $h$ of the Structure

Figure 2 summarizes the procedure used to identify the optimum parameter using an analytical approach and test. The objective of the procedure was the identification of the optimum  $Z_p$  and  $h$ . As an analytical approach, the time domain SSI analysis by the state space equation (SSE) was adopted and dynamic centrifuge tests were performed at the 20 g level.

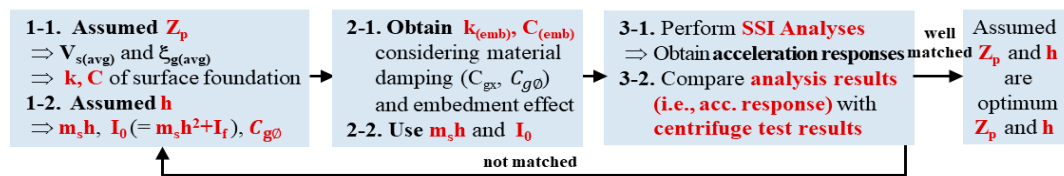


Figure 2. Procedure used to evaluate the optimum  $Z_p$  and  $h$  values of the structure.

## 3. Testing and Analysis Programs

### 3.1. Dynamic Centrifuge Tests

The dynamic centrifuge model tests were performed to obtain the seismic responses of the soil–structure system and to evaluate the optimum SSI parameters. As depicted in Figure 3b, the experimental model consists of a soft sandy soil, a shallow foundation, and a Single Degree of Freedom (SDOF) structure. The beam-type centrifuge facility in the Korea Advanced Institute of Science and Technology (KAIST) and KAIST Analysis center for Research Advancement (KARA) was used in this study, and the radius and maximum payload capacity of the facility were 5 m and 240 g-tons, respectively [8]. This facility was equipped with a shaking table that operated in flight conditions that could generate maximum horizontal acceleration of 40 g in model scale. The equivalent shear beam (ESB) soil container that consists of 10 aluminum alloy rectangular frames was mounted on the shaking table. The dynamic performance of the ESB box corresponded to that of ground motion and it was validated by Lee et al. [23]. The internal dimensions of the ESB box were 0.49 m × 0.49 m × 0.6 m at the model scale, and correspond to the dimensions of 9.8 m × 9.8 m × 12.0 m at the 20 g prototype scale. Figure 3b shows the ESB box soil–structure system mounted on the shaking table. All the dimensions were expressed in the form of a prototype scale according to the scaling law of the centrifuge model test [24]. In this study, eight cases (=four structures × two input motions/structure) of dynamic centrifuge tests were conducted.

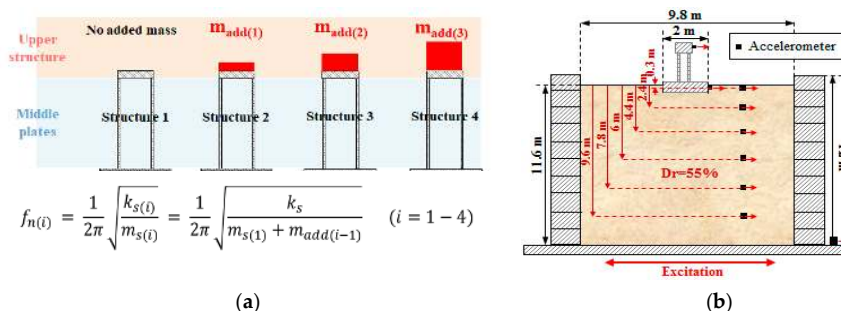


Figure 3. Model structures and tested soil–structure system: (a) Model structures for impact hammer tests, and (b) tested soil–structure system.

### 3.2. Analytical Approach Based on State Space Equation (SSE)

A time-domain analysis by the State Space Equation (SSE) has been used for the estimation of the dynamic structural response or system identification [11,25,26], and the analytical approach in this study was implemented using MATLAB R2014b. Equation (1) can be expressed as Equation (7) and the equation was converted to continuous-time SSE (Equation (8)), wherein  $Y$  in  $\{X\}$  consists of  $u_s$ ,  $u_x$ , and  $\phi$ . The discrete-time SSE of Equation (9) can be constructed by considering the general solution of Equation (8) and discrete-time interval ( $\Delta t$ ). At this point, continuous matrices  $[A]$  and  $[B]$  can be easily converted to discrete matrices  $[A_d]$  and  $[B_d]$  with MATLAB's `c2d` command [27–29]. In the discrete SSE, a sufficiently small-time interval ( $\Delta t$ ) setting was required because the constant  $U$  in  $\Delta t$  must be satisfied, and the stability of the system also needs to be secured [29]. Therefore, in this study, we used  $\Delta t = 5$  ms.

$$[M_A]\{\ddot{U}\} + [C_A]\{\dot{U}\} + [K_A]\{U\} = -\ddot{x}_g\{M_B\} \quad (7)$$

$$\begin{Bmatrix} \dot{Y} \\ \dots \\ \ddot{Y} \end{Bmatrix} = \begin{bmatrix} 0 & \vdots & I \\ \dots & \dots & \dots \\ -M_A^{-1}K_A & \vdots & -M_A^{-1}C_A \end{bmatrix} \begin{Bmatrix} Y \\ \dots \\ \dot{Y} \end{Bmatrix} + \begin{Bmatrix} 0 \\ \dots \\ -M_A^{-1}\{M_B\} \end{Bmatrix} \ddot{x}_g \Rightarrow \{\dot{X}\} = [A]\{X\} + [B]\{U\} \quad (8)$$

$$\{X_{i+1}\} = [A_d]\{X_i\} + [B_d]\{U_i\} \quad (9)$$

Based on Equation (9),  $\{X_{i+1}\} = \{Y_{i+1} : \dot{Y}_{i+1}\}^T$  was obtained in a step-by-step manner, and the relative acceleration response  $\{\ddot{Y}\} = \{\ddot{u}_s, \ddot{u}_x, \ddot{\phi}\}^T$  was then calculated according to Equation (10). Finally, the absolute acceleration response of the superstructure and the foundation  $\{\ddot{x}_s, \ddot{x}_f\}$  was determined based on Equation (11).

$$\{\ddot{Y}\} = \begin{Bmatrix} -M_A^{-1}K_A & \vdots & -M_A^{-1}C_A \end{Bmatrix} \begin{Bmatrix} Y \\ \vdots \\ \dot{Y} \end{Bmatrix}^T + \{-M_A^{-1}\{M_B\}\} \ddot{x}_g = \begin{Bmatrix} \ddot{u}_s & \ddot{u}_x & \ddot{\phi} \end{Bmatrix}^T = \begin{Bmatrix} -M_A^{-1}K_A & \vdots & -M_A^{-1}C_A \end{Bmatrix} \begin{Bmatrix} u_s & u_x & \phi \\ \vdots & \dot{u}_s & \dot{u}_x & \dot{\phi} \end{Bmatrix}^T + \{-M_A^{-1}\{M_B\}\} \ddot{x}_g \quad (10)$$

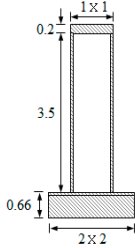
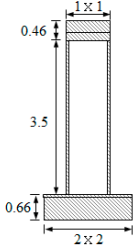
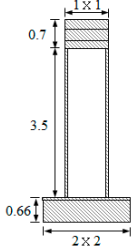
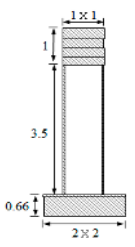
$$\begin{Bmatrix} \ddot{x}_s \\ \ddot{x}_f \end{Bmatrix} = \begin{bmatrix} 1 & 1 & h \\ 0 & 1 & 0 \end{bmatrix} \begin{Bmatrix} \ddot{u}_s \\ \ddot{u}_x \\ \ddot{\phi} \end{Bmatrix} + \begin{Bmatrix} 1 \\ 1 \end{Bmatrix} \ddot{x}_g \quad (11)$$

### 3.3. Properties of Structure in Tests and Analytical Approach

Four SDOF structural models made of steel were used. Each structural model consisted of (1) a lumped mass at the top position (i.e., upper structure,  $m_u$ ), (2) two thin plates (i.e., middle plates,  $m_m$ ) below the lumped mass considered to show shear deformation, and (3) a direct mat foundation (i.e., lower structure,  $m_f$ ) at the bottom. To obtain the characteristics of the structure for the time domain SSI analyses, impact hammer tests were performed on four structures with the exception of all the lower structures subject to the fixed-base condition. Accordingly, acceleration time history (ATH) data were acquired. The natural frequency ( $f_{ni}$ ) of each system was then obtained based on the fast Fourier transformation (FFT), and the relationship between  $f_{ni}$  and added mass ( $m_{\text{add}(i-1)}$ ) of each model structure was formulated. Finally, the effective lateral stiffness ( $k_s$ ) and effective mass of the superstructure ( $m_s$ ) were estimated based on the nonlinear curve fitting of the data with the use of the natural frequency formula of SDOF shown in Figure 3a. As the massless beam was considered in the 3DOF time domain SSI analysis,  $m_f$  was calculated by subtracting the  $m_s$  from the total mass of the structure ( $m_t$ ) that was defined as  $m_t = m_u + m_m + m_l = m_s + m_f$ . Given that the damping ratio of the structure cannot be obtained analytically, it is determined through free vibration tests [30]. The scaling factor  $N$  (prototype/model) is 20 because the centrifugal acceleration in each test is 20 g. The obtained

results are listed in Table 4. The width of the square footing is 2 m, and the effective radius  $r$  ( $= r_x \cong r_\phi$ ) was calculated as 1.135 m.

**Table 4.** Dimensions and properties of each structural model at the prototype scale.

Structure Models	Structure 1	Structure 2	Structure 3	Structure 4
dimensions (m)				
mass of upper structure ( $m_u$ , kg)	1580	3634	5530	7900
mass of middle plates ( $m_m$ , kg)		1991		
mass of lower structure ( $m_l$ , kg)		20,856		
natural frequency ( $f_{ni}$ , Hz)	3615	2540	2097	1773
effective mass of superstructure ( $m_s$ , kg)	2003	4057	5953	8323
effective mass of foundation. ( $m_f$ , kg)		22,424		
effective lateral stiffness ( $k_s$ , N/m)		1,033,191		
damping ratio ( $\xi_s$ , %)	1.406	1.674	2.379	2.252

Note: As the mass of the superstructure increases, the natural frequency clearly decreases, but the tendency of damping ratio increase is unclear.

### 3.4. Soil Properties and Ground Condition in Tests and Analytical Approaches

Dry silica sand layers were prepared with a relative density ( $D_r$ ) of 55% by using sand rainer. The properties of silica sand are listed in Table 5, and the  $V_s$  profiles are shown in Figure 4a. In this case, USCS is the unified soil classification,  $D_{50}$  is the median particle size,  $G_s$  is the specific gravity,  $e_{max}$  is the maximum void ratio,  $e_{min}$  is the minimum void ratio,  $\gamma_d$  is the dry unit weight of the soil,  $\phi$  is the internal friction angle of the soil, and  $K_0$  is the calculated coefficient of the earth pressure at rest based on Jacky's formula (i.e.,  $K_0 = 1 - \sin\phi$ ). Kim et al. [31] obtained the  $V_s - \sigma'_v$  profile by performing in-flight bender element tests on the silica sand with the relative densities of 40% and 80%. In this study, the  $V_s - \sigma'_v$  profile was obtained by interpolating the results of Kim et al. [31]. Finally, the  $V_s - Z$  profile was acquired based on the  $Z = \sigma'_v / \gamma_d$  relationship. Resonant column tests were performed with mean effective stress values  $\sigma'_m = 25, 50, \text{ and } 100 \text{ kPa}$ , and the results were used in one-dimensional equivalent SRAs, as shown in Figure 4b, wherein  $G/G_{max} - \log\gamma$  is the modulus reduction curve of the soil,  $\xi_g - \log\gamma$  is the damping ratio curve of the soil and  $\sigma'_m$  is the mean effective stress that can be calculated as  $(1 + 2K_0)\sigma'_v/3$ .

**Table 5.** Properties of silica sand used in this study and ground condition.

General Properties [32]					Ground Condition			
USCS	$D_{50}$ (mm)	$G_s$	$e_{max}$	$e_{min}$	$D_r$ (%)	$\gamma_d$ (kN/m <sup>3</sup> )	$\phi$ (°)	$K_0$
SP	0.22	2.65	1.130	0.611	55	14.092	37	0.398



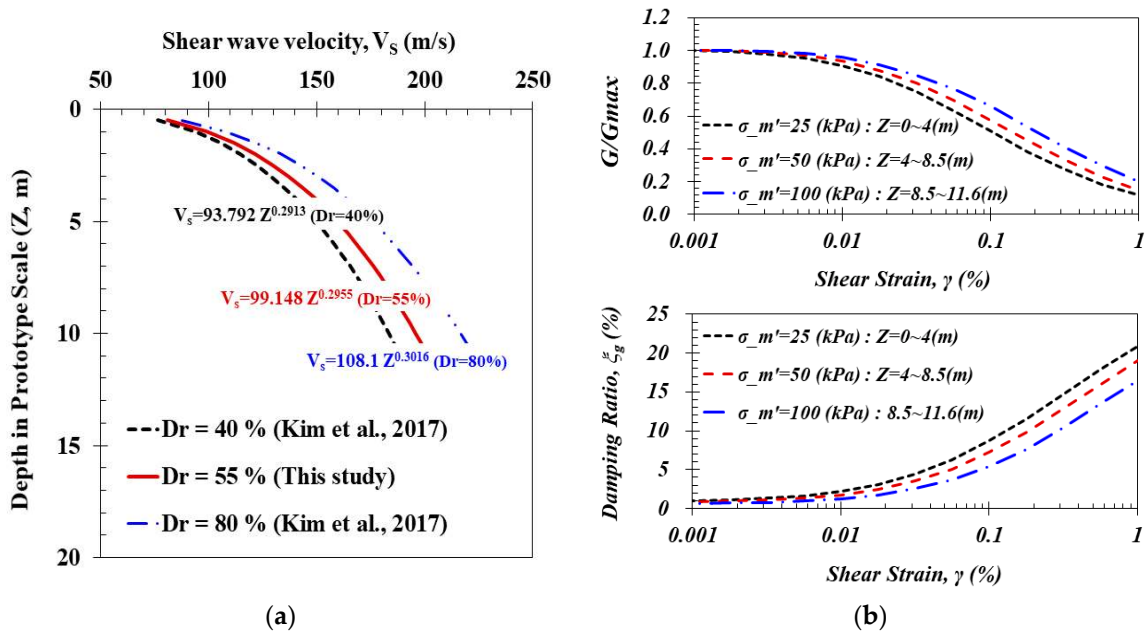


Figure 4. vs. profile and resonant column test results: (a)  $V_s$ - $Z$  relationship and (b) modulus reduction and damping curves.

### 3.5. Input Motions in Tests and Analyses

In this study, three input motions were used for tests and analyses: (1) Hachinohe earthquake motion with abundant low-frequency contents, (2) Northridge earthquake motion with abundant high-frequency contents, and (3) synthesized motion that consisted of 2, 6, and 10 Hz sinusoidal waves. Figure 5 is normalized Fourier amplitude spectra showing the frequency characteristics of each representative input motion. The characteristics of each motion type, including peak ground acceleration (PGA), are summarized in Table 6, wherein  $f_i$  contains every frequency of the Fourier amplitude spectrum that ranges from 0.25 to 20 Hz ( $\Delta f \leq 0.05$  Hz),  $A_i$  is the Fourier amplitude, and the parameter  $f_m$  is the reciprocal of the mean period ( $T_m$ ) suggested by Rathje et al. [33] and used as a representative frequency motion index.

Base motions were the measured outcrop motions at the outer bottom of the centrifuge test box and were used to SRAs. Free-field motions (FFMs) were measured as within motions at half the embedment depth of the foundation (i.e.,  $Z = 0.3$  m) and were used for analytical approach (i.e., 3DOF SSI analyses).

$$T_m = \sum_{i=1}^n \left( \frac{A_i^2}{f_i} \right) / \sum_{i=1}^n A_i^2, \quad f_m = \frac{1}{T_m} \quad (12)$$

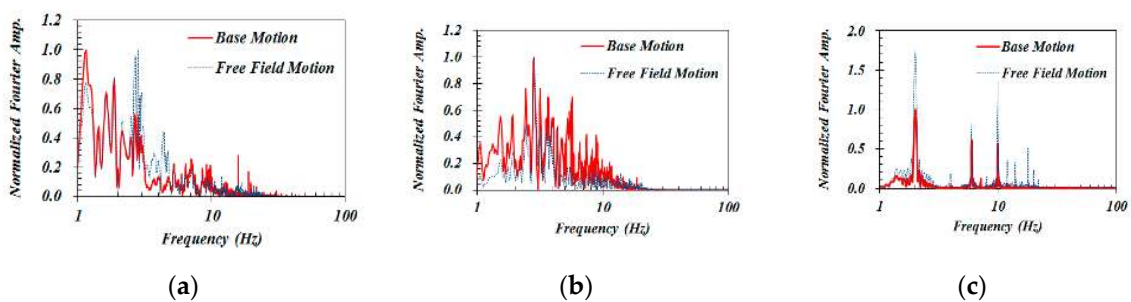


Figure 5. Frequency contents of the motions at base and free field: (a) Hachinohe IV, (b) Northridge II, and (c) Synthesized I.

**Table 6.** Characteristics of base and free-field motions used in this study.

Case	Input Motion	Base Motions		Free Field Motions	
		PGA (g)	$f_m$ (Hz)	PGA (g)	$f_m$ (Hz)
structure 1	Hachinohe I	0.112	1.842	0.227	2.268
structure 2	Hachinohe II	0.245	1.685	0.573	2.215
structure 3	Hachinohe III	0.283	1.637	0.585	2.157
structure 4	Hachinohe IV	0.113	1.797	0.193	2.194
<b>Average value</b>		0.188	1.740	0.395	2.209
structure 1	Northridge I	0.119	3.355	0.285	3.564
structure 3	Northridge II	0.315	3.353	0.609	3.166
<b>Average value</b>		0.217	3.354	0.447	3.365
structure 2	Synthesized I	0.188	2.814	0.317	3.394
structure 4	Synthesized II	0.189	2.887	0.345	3.167
<b>Average value</b>		0.189	2.851	0.331	3.281

Note: The mean frequency of each input motion follows the order: Hachinohe < Synthesized < Northridge.

#### 4. Determination of Soil–Spring Constant and Damping Coefficient

##### 4.1. Site-Response Analyses (SRAs) and Strain-Independent Soil Properties

One dimensional equivalent linear SRAs, One of the methods that can be used to obtain the acceleration response of the soil layer and to obtain the equivalent linear soil properties, were conducted to obtain strain-independent  $V_s$  and  $\xi_g$  values with the program STRATA that was developed by Kottke and Rathje [34]. Figure 6a shows that the ATHs from SRAs match well those from the test results at  $Z = 0.3$  m, and Figure 6b,c shows the equivalent  $V_s$  and  $\xi_g$ -depth results (i.e., the strain-independent  $V_s$  depth and  $\xi_g$ -depth relationships) at their final effective shear strain values.

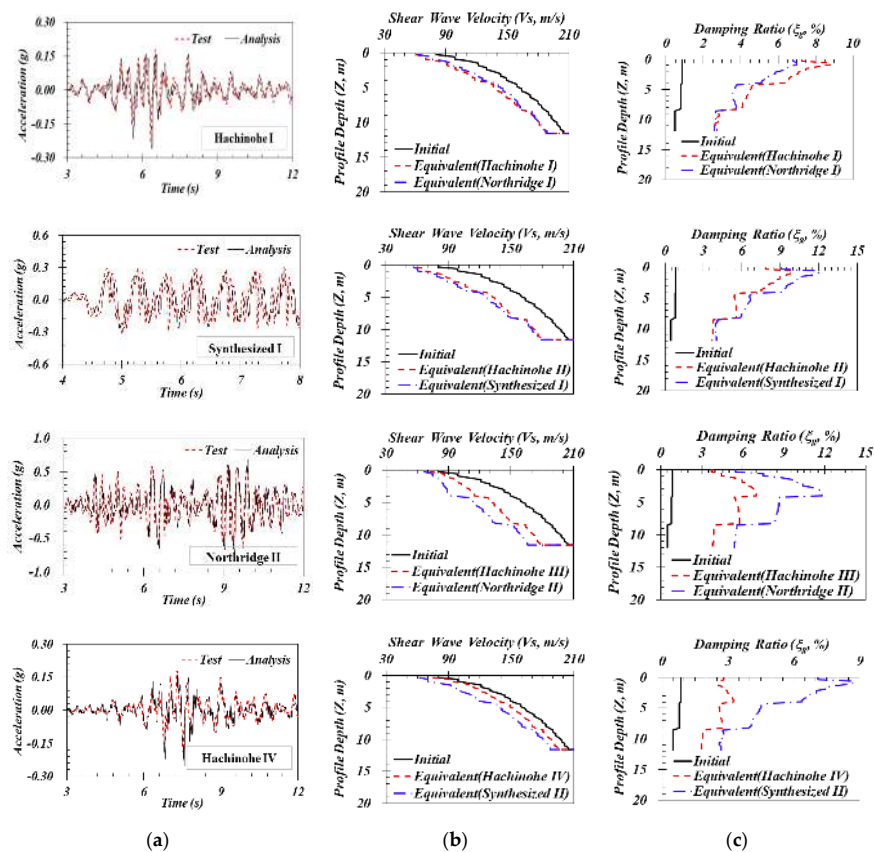


**Figure 6.** Equivalent  $V_s$  and  $\xi_g$  values obtained by the SRAs: (a) Acceleration time history, (b) equivalent  $V_s$  value, and (c) equivalent  $\xi_g$  value.

#### 4.2. Depth-Independent Soil Properties

Figure 7 shows the variations of  $V_s$  and  $\xi_g$  that are converted to their depth-independent forms using Equation (2), and are based on three types of  $Z_p$  scenarios. Regarding the effective radius  $r$  in square footing,  $r_x = 0.56 B$  in the swaying mode is similar to  $r_\phi = 0.57 B$  in the rocking mode, and the effective profile depth  $Z_p$  is normalized with one effective radius  $r$  (i.e.,  $r = 0.565 B$ ). In addition,  $Z_p/r = 0.75, 2$ , and  $4$ , correspond to  $Z_p = 0.85, 2.3$ , and  $4.5$  m, respectively.

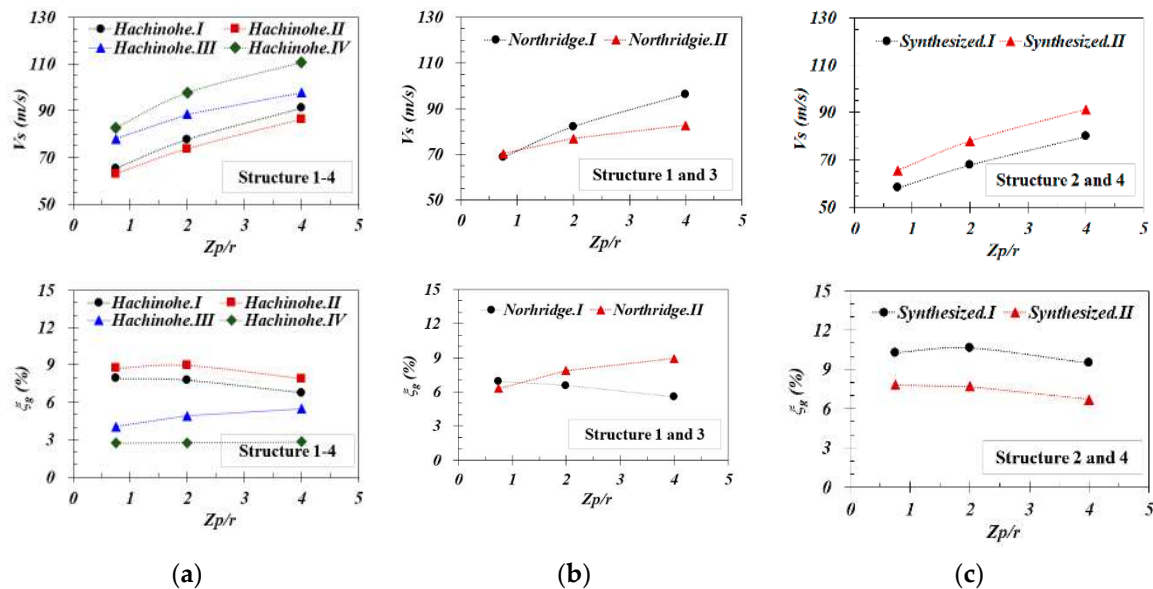


**Figure 7.** Variations of strain- and depth-independent  $V_s$  and  $\xi_g$  values for the soil for each ground motion case: (a) Hachinohe, (b) Northridge, and (c) synthesized.

### 5. Evaluation of Two Optimum SSI Parameters $Z_p$ and $h$

#### 5.1. Determination of Analysis CASES Considering the SSI Parameters

The soil–spring constant and damping coefficient depend on  $V_s$  and  $\xi_g$  as well as on the foundation conditions (e.g., geometry of foundation, embedded depth, and other subsoil properties) as follows

- $k_{h(emb)}$  and  $k_{r(emb)} = f(\rho, V_s, \text{geometry of foundation}, \nu, D)$
- $C_{h(emb)}$  and  $C_{r(emb)} = f(\rho, V_s, \text{geometry of foundation}, \nu, D, \xi_g, m_t \text{ or } I_0)$

$V_s$  and  $\xi_g$  are determined by the effective profile depth and  $I_0$  determined by the effective height affects  $C_{g\phi}$ . Given that  $h$  and  $Z_p$  affect the soil–spring constants and damping coefficients, the number of the analysis cases were set as follows:

- In the case of the optimum  $h$  value: 24 soil-spring constants and damping coefficients = one formula  $\times$  eight input motions  $\times$  three effective heights  $\times$  one effective profile depth
- In the case of the optimum  $Z_p$  value: 48 soil-spring constants and damping coefficients = two formulas  $\times$  eight input motions  $\times$  one effective height  $\times$  three effective profile depths

#### 5.2. Quantification of Differences between Test and Analysis Results

To evaluate the differences in phase, amplitude, frequency contents, and amplification characteristics between the test and analysis results, the mean squared errors (MSEs) for ATH and response spectrum (RS) of each superstructure were obtained in the forms of  $MSE_{TH}$  and  $MSE_{RS}$ , respectively, and their sums (i.e.,  $\sum MSE_i$ ) were used to comprehensively evaluate the conformity of the analysis to the test results. In Equations (13) to (15),  $a_{test(k)}$  and  $a_{anal(k)}$  were the acceleration

responses of the test and analysis at a certain time  $t = k$ , and  $SA_{test(j)}$  and  $SA_{anal(j)}$  were the spectral acceleration values of the test and analyses at a certain frequency  $f = j$ , respectively. When the value of  $\sum MSE_i$  is small, the overall agreement between the test and analysis results is better.

$$MSE_{TH} = \frac{1}{n} \sum_{i=1}^n (a_{test(k)} - a_{anal(k)})^2 \quad (13)$$

$$MSE_{RS} = \frac{1}{n} \sum_{i=1}^n (SA_{test(j)} - SA_{anal(j)})^2 \quad (14)$$

$$\sum MSE_i = MSE_{TH} + MSE_{RS} \quad (15)$$

### 5.3. Evaluation of the Optimum $h$

To evaluate the optimum effective height ( $h$ ), 24 analyses were conducted in total (i.e., 24 cases = four structures  $\times$  two input motions/structure  $\times$  three effective heights), where  $Z_p/r = 4$  (i.e.,  $Z_p = 4.5$  m). The Richart and Lysmer formula was considered for the analyses. In each case, the minimum  $h$  value corresponds to the base to  $m_s$  case, and the maximum  $h$  value to the moment equilibrium case. As  $h$  changes,  $I_0$  and  $m_s h$  also changes in all the analysis cases. The analysis cases are summarized in Table 7, wherein no case matched the  $I_0$  and  $m_s h$  condition simultaneously. The shaded area denoted the case matching of each property of the prototype structure (i.e.,  $I_0$  or  $m_s h$ ).

**Table 7.** Analysis cases for the evaluation of the optimum  $h$  value.

Structure	Input Motion/PGA (g)	Condition of $h$	$h$ (m)	$I_0$ (t·m <sup>2</sup> )	$m_s h$ (t·m)
structure 1	Hachinohe I/0.227 Northridge I/0.285	base to $m_s$	4.260	47.072	8.531
		Mass Moment of Inertia compatible	4.561	52.388	9.134
		moment equilibrium	5.499	71.276	11.011
structure 2	Hachinohe II/0.573 Synthesized I/0.317	base to $m_s$	4.390	88.909	17.808
		Mass Moment of Inertia compatible	4.530	93.979	18.377
		moment equilibrium	4.988	111.653	20.234
structure 3	Hachinohe III/0.585 Northridge II/0.609	base to $m_s$	4.510	131.806	26.846
		Mass Moment of Inertia compatible	4.601	136.745	27.388
		moment equilibrium	4.909	154.172	29.221
Structure 4	Hachinohe IV/0.193 Synthesized II/0.345	base to $m_s$	4.660	191.46	38.783
		Mass Moment of Inertia compatible	4.724	196.448	39.315
		moment equilibrium	4.938	213.642	41.094

Figure 8 shows the ATHs and  $\sum MSE_i$  values of the test and analysis results. According to the results of the analysis, as  $h$  increases,  $\sum MSE_i$  increases. Based on the tendency and calculation result of  $\sum MSE_i$ ,  $\sum MSE_i$  at  $h_{base\ to\ m_s}$  yielded a minimum error of 0.106 on average,  $\sum MSE_i$  at  $h_{MMI}$  yielded an error of 0.127 on average, and  $\sum MSE_i$  at  $h_{moment}$  yielded the greatest error of 0.229 on average. Given that  $\sum MSE_i$  at  $h_{base\ to\ m_s}$  was estimated to be lower than that at full height,  $h_{base\ to\ m_s}$  was considered as the optimum effective height.

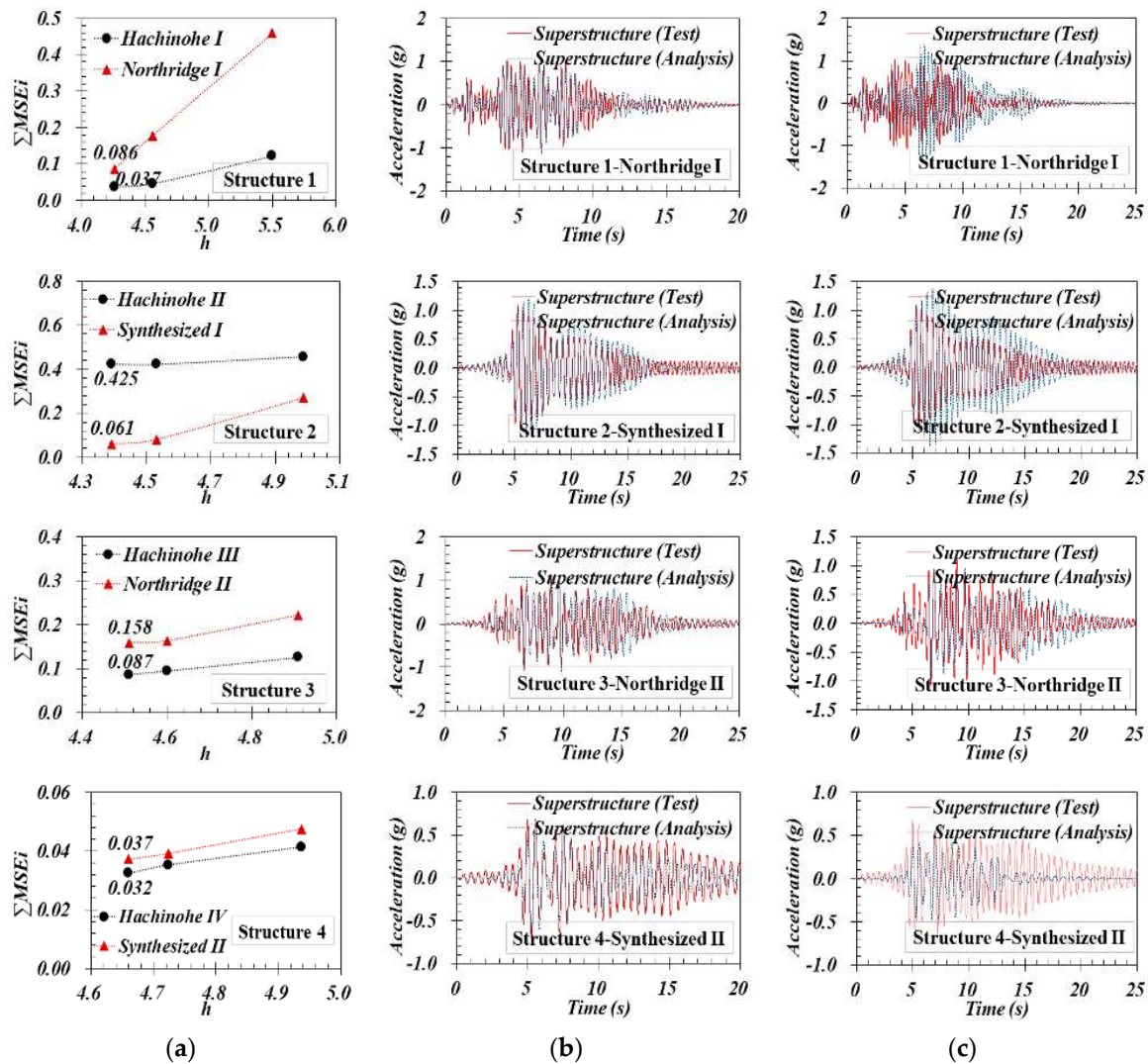


**Figure 8.** Differences between tests and analyses, and acceleration time history (ATHs) of all tested cases: (a)  $\sum MSE_i$  values comparisons of test and analysis data, (b) ATH at  $h_{base\ to\ m_s}$ , and (c) ATH at  $h_{moment}$ .

#### 5.4. Evaluation of the Optimum Effective Profile Depth $Z_p$

In the evaluation of the optimum effective profile depth ( $Z_p$ ), 48 analyses were conducted in total (i.e., 48 cases = four structures  $\times$  two input motions/structure  $\times$  three effective profile depths  $\times$  two types of formulas), wherein the embedment correction factor suggested by Whitman [6] and  $h_{base\ to\ m_s}$  was used in common. The analysis cases are summarized in Table 8.

Figure 9 shows the  $\sum MSE_i$  value of each analysis case, and Table 9 lists the maximum acceleration responses of the superstructure, wherein the shaded areas represent the analysis cases that best match the test results (i.e., the case with the minimum  $\sum MSE_i$ ). Although two analysis cases (i.e., structure 3-Northridge II and structure 4-Synthesized II) show that the maximum acceleration responses were smaller than those of the corresponding test results, the differences were not considerable.

Specifically, the maximum acceleration responses of the conducted analyses were 93.2% and 99.0% compared with those of the corresponding test results. The average values of  $\sum MSE_i$  in the case at which Wolf’s formula was used was 0.098, and the average value of  $\sum MSE_i$  in the case at which Richart and Lysmer’s formula was used was 0.106. Thus, the difference of  $\sum MSE_i$  between the results of the two formulas was not significant. In terms of the maximum acceleration response, the results generated by Richart and Lysmer’s formula were found to be 0.8–12.4% more conservative than those obtained based on Wolf’s formula, as listed in Table 9. In terms of the input motion, the average value of  $\sum MSE_i$  was 0.137 for the Hachinohe motion, 0.124 for Northridge motion, and 0.045 for synthesized motion. These findings show that the analysis results based on the use of the seismic wave were associated with a larger error compared with that obtained based on the analysis with the use of synthesized motion. In all the tested cases, the acceleration response of the superstructure at  $Z_p/r = 0.75$  yielded a higher discrepancy between tests and analysis outcomes (i.e., the maximum  $\sum MSE_i$  value in all the cases of  $Z_p/r = 0.75$  was 2.403) but the responses at  $Z_p/r = 4$  showed good agreement (i.e., maximum  $\sum MSE_i$  in all the cases of  $Z_p/r = 4$  was 0.425).

Table 8. Analysis cases used to evaluate the optimum  $Z_p$  value.

Structure	Input Motions/PGA (g)	h (m)	$Z_p$ (m)	Formulas on k and C of Soil
structure 1	Hachinohe I/0.227 Northridge I/0.285	4.26		
structure 2	Hachinohe II/0.573 Synthesized I/0.317	4.39	0.85 (0.75 r) 2.3 (2 r) 4.5 (4 r)	Wolf [1] Richart and Lysmer [2] embedment correction factor–Whitman [6]
structure 3	Hachinohe III/0.585 Northridge II/0.609	4.51		
structure 4	Hachinohe IV/0.193 Synthesized II/0.345	4.66		

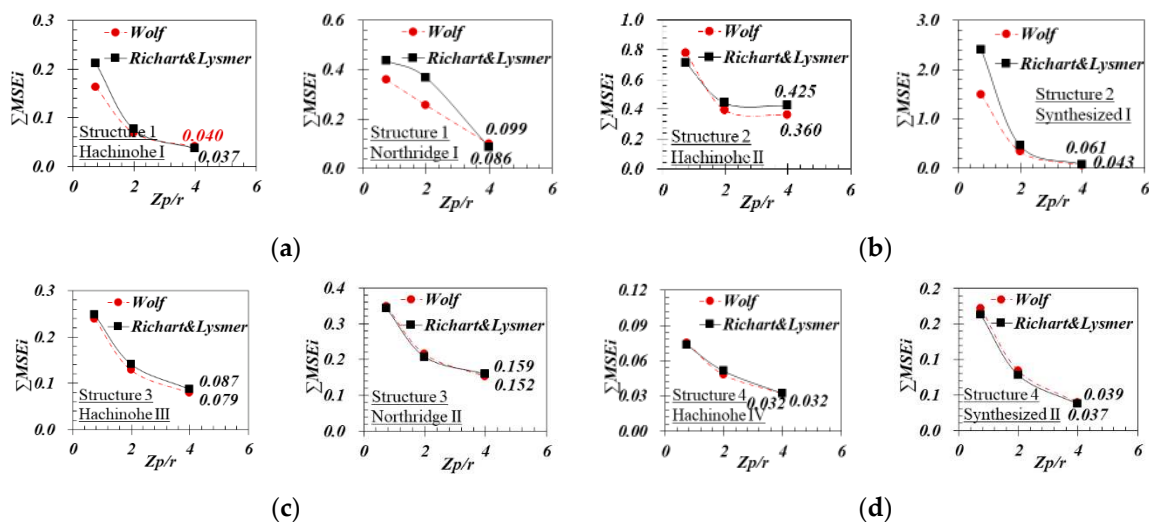
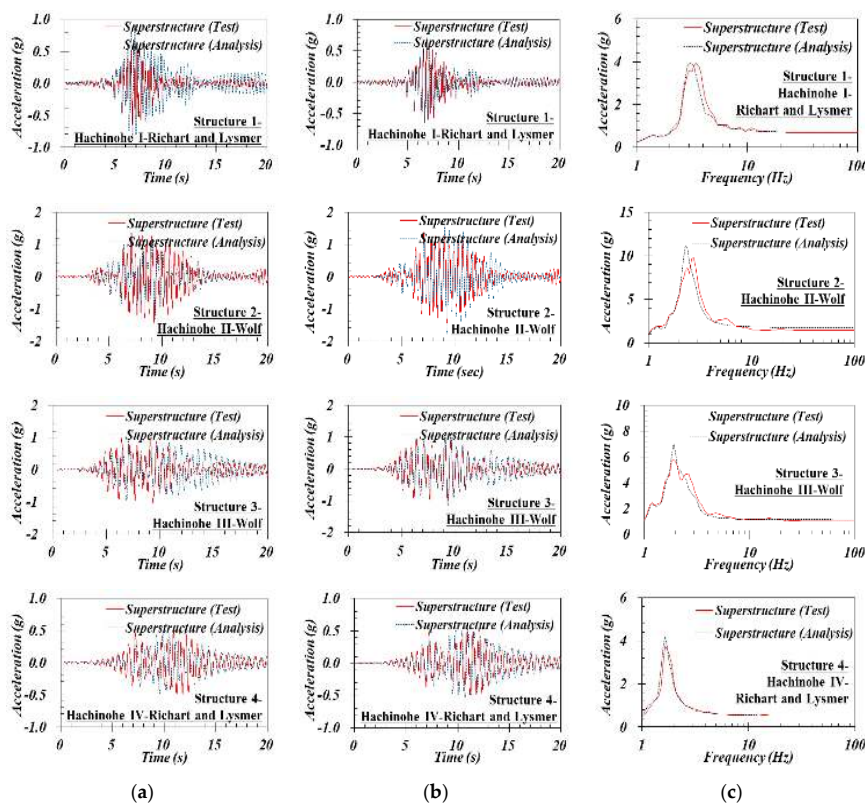


Figure 9. Difference between tests and analyses at each case: (a) Structure 1, (b) structure 2, (c) structure 3, and (d) structure 4.

**Table 9.** Comparison of test and analysis results in terms of maximum acceleration response at  $m_s$ .

		Analysis Results (g) $Z_p/r=0.75$						
Structure	Input Motion	Test (g)	Wolf's Formula			Richart and Lysmer's Formula		
			$Z_p/r=0.75$	$Z_p/r=2$	$Z_p/r=4$	$Z_p/r=0.75$	$Z_p/r=2$	$Z_p/r=4$
structure 1	Hachinohe I	0.685	0.885	0.785	0.694	0.941	0.812	0.707
	Northridge I	1.088	1.163	1.400	1.124	1.255	1.490	1.136
structure 2	Hachinohe II	1.454	1.304	1.725	1.772	1.352	1.798	1.803
	Synthesized I	1.100	1.707	1.383	1.173	1.919	1.449	1.213
structure 3	Hachinohe III	1.039	1.189	1.088	1.149	1.221	1.108	1.180
	Northridge II	1.150	0.991	1.040	1.072	0.999	1.051	1.097
structure 4	Hachinohe IV	0.521	0.469	0.517	0.515	0.488	0.529	0.526
	Synthesized II	0.702	0.540	0.589	0.687	0.562	0.603	0.695

Figure 10 shows the variations of the ATHs and RS of the superstructure during Hachinohe motion. The tendency to increase or decrease the maximum acceleration of the superstructure as the effective profile depth increases is unclear, but as the effective profile depth increases,  $\sum MSE_i$  clearly decreases, thus yielding the lowest value at  $Z_p/r = 4$ . Therefore, based on all the results in this study, it can be concluded that 4 r is the optimum effective profile depth.



**Figure 10.** Acceleration time histories and response spectra from tests and analyses: (a) ATHs at  $Z_p/r = 0.75$ , (b) ATHs at  $Z_p/r = 4$ , and (c) RS at  $Z_p/r = 4$ .

## 6. Conclusions

In this study, dynamic centrifuge tests and LDP-based analyses (i.e., time domain SSI analyses by SSE) were performed to evaluate the optimum effective height and effective profile depth conditions proposed in the conventional standards and prior research publications. Four structures and three ground motions were used in the centrifuge tests, and three effective heights and three effective profile depth conditions were considered as the SSI analysis cases in addition to the aforementioned test conditions. The main results of this research are summarized as follows.

1. In this study, the applicability of the SSI parameters suggested by various standards and studies was discussed, and the optimum SSI parameter selection procedure that (a) comprehensively considered the SSI parameters, (b) adopted an analytical approach and a physical model test, was suggested. Based on the established procedure, the optimum values of two controversial SSI parameters (i.e., the effective height and effective profile depth) were determined
  - Unlike the conventional standards that apply a simplified reduction factor for the initial shear wave velocity profile and do not apply any corrections in initial damping ratio profile, one dimensional equivalent linear site response analyses were performed to accurately obtain the equivalent strain-independent shear wave velocity ( $V_s$ ) and damping ratio ( $\xi_g$ ) of the soil. The equivalent  $V_s$  and  $\xi_g$  values that varied with depth obtained herein were converted to depth independent  $V_s$  and  $\xi_g$  values based on considerations of the effective profile depth ( $Z_p$ ).
  - Unlike the conventional research efforts that ignored soil material damping and indirectly determined soil damping based on the effective period lengthening ratio, the total soil damping was obtained directly by the addition of soil material damping to soil radiation damping. In addition, the stiffness and total damping of soil were determined based on embedded foundation conditions.
  - Unlike the conventional SDOF SSI analysis that was based on the RS, this study adopted a 3DOF time domain SSI analysis based on structural translation, foundation translation, and rocking behavior considerations to accurately obtain structural responses.
2. The effective height of the structure affected the rocking behavior of the soil–structure system (i.e.,  $m_s h$  and  $C_{g\varnothing}$ ). In this study, applicability of the following three effective height scenarios were evaluated based on the following test and analysis results: (1) Height from the bottom of the foundation to the center of the mass of the superstructure, and (2) height compatible to the total mass moment of inertia, and (3) height to satisfy moment equilibrium. As the effective height increased within the effective height range used in the analysis, the differences between test and analysis results increased. Consequently, in all the cases, the height from the bottom of the foundation to the center of the mass of the superstructure was the optimum effective height with the lowest  $\sum MSE_i$  value.
3. The optimum effective profile depth ( $Z_p$ ) was determined. This was used to average the dynamic soil property that varied as a function of depth. Three scenarios were considered in the analyses: (1)  $Z_p/r = 0.75$ , (2)  $Z_p/r = 2$ , and (3)  $Z_p/r = 4$ . As a result, 4 r was found to be the optimum effective profile depth with the lowest difference between the test and analysis results. In addition, the results associated with earthquake motions yielded higher errors than those of synthesized motions that consisted of sinusoidal waves at the frequencies of 2, 6, and 10 Hz. The maximum acceleration responses by Richart and Lysmer’s formula was more conservative than those obtained with Wolf’s formula.

**Author Contributions:** Conceptualization and methodology, H.-U.K. and D.-S.K.; formal analysis, H.-U.K.; investigation, H.-U.K.; resources, D.-S.K. and J.-G.H.; data curation, H.-U.K. and J.-G.H.; validation, J.-G.H., K.-W.K. and D.-S.K.; writing—original draft preparation, H.-U.K.; writing—review and editing, J.-G.H. and K.-W.K.; supervision, D.-S.K.; project administration, D.-S.K.; funding acquisition, D.-S.K. All authors have read and agreed to the published version of the manuscript.



**Funding:** This research was funded by Korea Construction Engineering and Transport Development Collaboratory Management Institute (KOCED), Korea Advanced Institute of Science and Technology (KAIST) and KAIST Analysis center for Research Advancement (KARA).

**Acknowledgments:** This research was supported by Korea Construction Engineering and Transport Development Collaboratory Management Institute (KOCED), Korea Advanced Institute of Science and Technology (KAIST) and KAIST Analysis center for Research Advancement (KARA).

**Conflicts of Interest:** The authors declare no conflict of interest.

## References

1. Wolf, J. *Dynamic Soil-Structure Interaction*; Section 3.4 Introductory Example; Prentice Hall: Englewood Cliffs, NJ, USA, 1985; pp. 38–50.
2. Richart, F.; Hall, J.; Woods, R. *Vibrations of Soils and Foundations*; Prentice-Hall: Englewood Cliffs, NJ, USA, 1970.
3. Gazetas, G. *Foundation Engineering Handbook*, 2nd ed.; Fang, H.Y., Ed.; Chapter 15 Foundation Vibrations; Springer Science Business Media: New York, NY, USA, 1991.
4. Stewart, J.; Seed, R.; Fenves, G. *PEER-98/07: Empirical Evaluation of Inertial Soil Structure Interaction*; Pacific Earthquake Engineering Research (PEER) Center: Berkeley, CA, USA, 1998.
5. Wong, H.; Luco, J. Tables of impedance functions for square foundations on layered media. *Soil Dyn. Earthq. Eng.* **1985**, *4*, 64–81. [[CrossRef](#)]
6. Whitman, R. *Soil Publications No-300: Analysis of Soil-Structure Interaction: A State-of-the-Art Review*; Massachusetts Institute of Technology: Cambridge, MA, USA, 1972.
7. Stewart, J.; Kim, S.; Bielak, J.; Dobry, R.; Power, M. Revisions to soil-structure interaction procedures in NEHRP design provisions. *Earthq. Spectra* **2003**, *19*, 677–696. [[CrossRef](#)]
8. Kim, D.; Lee, S.; Kim, D.; Choo, Y.; Park, H. Rocking effect of a mat foundation on the earthquake response of structures. *J. Geotech. Geoenviron. Eng.* **2015**, *141*, 10:04014085. [[CrossRef](#)]
9. Ko, K.; Ha, J.; Park, H.; Kim, D. Comparison between cyclic and dynamic rocking behavior for embedded shallow foundation using centrifuge tests. *Bull. Earthq. Eng.* **2018**, *16*, 5171–5193. [[CrossRef](#)]
10. Gavras, A.; Kutter, B.; Hakhamaneshi, M.; Gajan, S.; Tsatsis, A.; Sharma, K.; Kohno, T.; Deng, L.; Anastasopoulos, I.; Gazetas, G. Database of rocking shallow foundation performance: Dynamic shaking. *Earthq. Spectra* **2020**, *36*, 960–982. [[CrossRef](#)]
11. Kim, D.; Park, H.; Kim, D.; Lee, H. Nonlinear system identification on shallow foundation using Extended Kalman Filter. *Soil Dyn. Earthq. Eng.* **2020**, *128*, 105857. [[CrossRef](#)]
12. FEMA. *Prestandard and Commentary for the Seismic Rehabilitation of Buildings (FEMA 356)*; Federal Emergency Management Agency: Washington, DC, USA, 2000.
13. ATC. *Seismic Evaluation and Retrofit of Concrete Buildings (ATC-40)*; Applied Technology Council: Redwood City, CA, USA, 1996.
14. FEMA. *Improvement of Nonlinear Static Seismic Analysis Procedures (FEMA 440)*; Federal Emergency Management Agency: Washington, DC, USA, 2004.
15. ASCE. *Seismic Evaluation and Retrofit of Existing Buildings (ASCE 41-13)*; Chapter 8 Foundations and Geologic Site Hazards; American Society of Civil Engineers: Reston, VA, USA, 2014.
16. BSSC. *NEHRP Recommended Provisions for Seismic Regulation for New Buildings and Other Structures*; Federal Emergency Management Agency: Washington, DC, USA, 1998.
17. Stewart, J.; Fenves, G.; Seed, R. Seismic Soil-Structure Interaction in Buildings. I: Analytical Methods. *J. Geotech. Geoenviron. Eng.* **1999**, *125*, 26–37. [[CrossRef](#)]
18. BSSC. *NEHRP Recommended Provisions for Seismic Regulations for New Buildings and Other Structures (FEMA 450-1 2003 Edition)*; Federal Emergency Management Agency: Washington, DC, USA, 2004.
19. EPRI. *1010808: Engineering Technical Training Modules for Nuclear Plant Engineers-Civil/Structural Series Module #5-Soil Structure Interaction*; EPRI: Palo Alto, CA, USA, 2005.
20. Mikami, A.; Sawada, T. Time-domain identification system of dynamic soil-structure interaction. In Proceedings of the 13th World Conference on Earthquake Engineering, Vancouver, BC, Canada, 1–6 August 2004. Paper No. 747.
21. ASCE. *Seismic Analysis of Safety-Related Nuclear Structures (ASCE 4-16)*; Chapter 5 Soil-Structure Interaction Modeling and Analysis; American Society of Civil Engineers: Reston, VA, USA, 2017; p. 24.

22. Chowdhury, I.; Dasgupta, S. *Dynamics of Structure and Foundation-A Unified Approach 2. APPLICATIONS*; Chapter 2, Analysis and Design of Machine Foundation—2.4 Effect of Embedment on Foundation; Taylor & Francis Ltd.: London, UK, 2009.
23. Lee, S.; Choo, Y.; Kim, D. Performance of an equivalent shear beam (ESB) model container for dynamic geotechnical centrifuge tests. *Soil Dyn. Earthq. Eng.* **2013**, *44*, 102–114. [[CrossRef](#)]
24. Taylor, R. *Geotechnical Centrifuge Technology*; Centrifuge in Modeling: Principle and Scale Effects; Taylor & Francis Ltd.: London, UK, 1995; pp. 19–33.
25. Chang, S.; Kim, D.; Kim, D.; Kang, K. Earthquake Response Reduction of Building Structures Using Learning-Based Lattice Pattern Active Controller. *J. Earthq. Eng.* **2012**, *16*, 317–328. [[CrossRef](#)]
26. Nica, G.; Calofir, V.; Corăci, I. A State Space Formulation for the Evaluation of the Pounding Forces During Earthquake. *Math. Model. Civ. Eng.* **2018**, *14*, 37–49. [[CrossRef](#)]
27. Karris, S. *Introduction to Simulink with Engineering Applications*; Chapter 5 The Discrete Blocks Library; Orchard Publications: Fremont, CA, USA, 2006; pp. 5–12.
28. Kalechman, M. *Practical MATLAB Basics for Engineers*; Chapter 7 Polynomials and Calculus, a Numerical and Symbolic Approach; Taylor & Francis Group LLC: Boca Raton, FL, USA, 2009; pp. 474–481.
29. Ross, P. *The handbook of Software for Engineers and Scientists*; Section V Engineering Tools, 55 MATLAB in Systems and Controls; Taylor & Francis Group: Boca Raton, FL, USA, 1996.
30. Chopra, A. *Dynamics of Structures*; Section 2.2.4 Free Vibration Tests; Prentice Hall: Upper Saddle River, NJ, USA, 2007.
31. Kim, J.; Choo, Y.; Kim, D. Correlation between the Shear-Wave Velocity and Tip Resistance of Quartz Sand in a Centrifuge. *J. Geotech. Geoenviron. Eng.* **2017**, *143*, 04017083. [[CrossRef](#)]
32. Cho, H.; Kim, N.; Park, H.; Kim, D. Settlement Prediction of Footings Using  $V_S$ . *Appl. Sci.* **2017**, *7*, 1105. [[CrossRef](#)]
33. Rathje, E.; Abrahamson, N.; Bray, J. Simplified frequency content estimates of earthquake ground motions. *J. Geotech. Geoenviron. Eng.* **1998**, *124*, 150–159. [[CrossRef](#)]
34. Kottke, A.; Rathje, E. *PEER-2008/10: Technical Manual for Strata*; Pacific Earthquake Engineering Research (PEER) Center: Berkeley, CA, USA, 2009.



© 2020 by the authors. Licensee MDPI, Basel, Switzerland. This article is an open access article distributed under the terms and conditions of the Creative Commons Attribution (CC BY) license (<http://creativecommons.org/licenses/by/4.0/>).